JOURNAL OF MATERIALS SCIENCE 31 (1996) 1501–1508

Analysis of phase transformation in Fe–C alloys using differential scanning calorimetry

G. P. KRIELAART, C. M. BRAKMAN, S. VAN DER ZWAAG
Laboratory of Materials Science, Delft University of Technology, Rotterdamseweg 137, 2628 AL Delft, The Netherlands

Differential scanning calorimetry (DSC) is a well suited technique for studying phase transformation kinetics provided the transformation involves some kind of heat effect. The diffusional transformation in Fe–C alloys and low alloy steels upon cooling from the austenitic state involve both heat of transformation and changes in heat capacity. In principle, it can therefore be analysed using DSC techniques. Particular complications in the analysis of the heat effects occurring on this transformation are the strong temperature dependence of the heat capacity of the ferrite and the strong temperature dependence of the enthalpy of formation of ferrite from austenite. A simple mathematical method is presented, which allows for the non-linear temperature dependence of heat capacities and enthalpy of formation. As a consequence, the method can be used to analyse the simultaneous formation of pearlite. Using this method, the fractions of both pro-eutectoid ferrite and pearlite as a function of the temperature are determined from heat capacity measurements for several Fe–C alloys. Data for the enthalpy of formation of pearlite are presented. The method presented is generally applicable for analysing reactions or transformations occurring over a wide temperature interval where the heat effects are temperature dependent.

1. Introduction

Differential scanning calorimetry (DSC) is a commonly used technique in the investigation of reaction and transformation kinetics in a wide range of materials including polymers, ceramics and metals. The theoretical background of this technique and the usual methods of analysis are described in several textbooks (e.g. Refs [1, 2]). Studying the kinetics of transformations usually requires the determination of the fractions transformed as a function of the time elapsed. In the case of DSC, the determination of reaction rates and fractions transformed involves the analysis of the behaviour of the DSC curve during the transformation. For this purpose, the part of the signal due to the heat of transformation must be separated from the part of the signal due to the intrinsic heat capacity of the sample itself. There are several methods to do this, each involving the partial area integration of the peak caused by the heat of transformation occurring during the transformation [1, 2]. These methods implicitly assume that the difference of the heat capacity between parent and product phase does not change during the phase transformation. If it does, some of the heat effects are interpreted as either heat of transformation or intrinsic heat capacity, depending on the change of the difference in heat capacity. In this case, the usual methods of analysis will not yield the true fraction transformed.

The technologically very important decomposition of austenite into ferrite in hypo-eutectoid Fe–C alloys and (low alloy) steels is a typical example of the latter class of transformations. The austenite decomposition is the most important step in controlling the microstructure, and hence the mechanical properties, of low-alloy construction steels. This transformation takes place when crossing the α/γ two-phase region of the Fe–C diagram on cooling from the one-phase austenitic state. At approximately 1040 K, ferrite exhibits a ferromagnetic transition, causing a strong nonlinear behaviour of the heat capacity of ferrite in a relatively wide temperature range, rendering partial area integration methods invalid. The formation of so-called pro-eutectoid ferrite is followed by a eutectoid reaction, pearlite formation, as soon as the remaining austenite has become supersaturated. This itself is also a reason why partial area integration methods cannot be used in this case. It is the purpose of this paper to demonstrate a new method for the determination of fractions transformed from DSC measurements in the case that non-linearities with respect to temperature of heat capacities and enthalpies of formation cannot be neglected.

2. Theory

In this section, a general method for the analysis of heat effects caused by phase transformations or

0022–2461

reactions will be presented. The transformation of austenite (γ) to ferrite (α) in Fe–C alloys, which occurs when crossing the α/γ two-phase region from the γ one-phase region, will serve as an example.

2.1. Analysis of heat effects

In general, when two phases α and γ are present in a sample of material, the experimentally measured heat capacity C_p is a weighted sum of the capacity of the two phases

$$C_p = x^\alpha C_p^\alpha + x^\gamma C_p^\gamma \quad (1)$$

The (molar or mass) fractions x^α and x^γ are related by

$$x^\alpha + x^\gamma = 1 \quad (2)$$

If, due to a phase transformation, an additional amount of heat is dissipated or generated by the sample, a term dQ/dT has to be added to the right hand side of Equation 1, thus correcting for this heat of transformation. It holds that [3]

$$\frac{dQ}{dT} = \Delta H^{\alpha/\gamma} \frac{dx^\gamma}{dT} \quad (3)$$

where $\Delta H^{\alpha/\gamma}$ is the enthalpy difference of both phases. Rewriting the extended form of Equation 1 yields

$$\frac{dx^\gamma}{dT} = \frac{C_p^\alpha - C_p^\gamma}{\Delta H^{\alpha/\gamma}} x^\gamma - \frac{C_p^\alpha - C_p}{\Delta H^{\alpha/\gamma}} \quad (4)$$

This equation holds as long as the decomposition of austenite into pro-eutectoid ferrite is the only process to be considered. In the analysis, C_p^α, C_p^γ, and $\Delta H^{\alpha/\gamma}$ are allowed to be functions of the temperature. The austenite and pro-eutectoid ferrite fractions can be determined as functions of temperature using Equation 4

The formation of a third phase during the transformation imposes a difficulty because the relation between the fractions is less clear as in the case where the transformation only involves formation of pro-eutectoid ferrite. On the formation of a third phase θ (in the case of Fe–C alloys: cementite), Equation 2 now becomes

$$x^\gamma + x^\alpha + x^\theta = 1 \quad (5a)$$

The eutectoid reaction $\gamma \rightarrow \alpha + \theta$ in Fe–C alloys leads to the formation of pearlite, a mixture of ferrite and cementite with a lamellar microstructure. According to the Fe–C equilibrium diagram, the ferrite and cementite fractions have a fixed ratio at completed transformation, depending mainly on the average carbon content (neglecting the very small temperature dependence of the carbon solubility in ferrite). However, due to kinetic reasons, the ratio between the ferrite and pearlite fractions is not fixed. It varies not only with the alloy carbon content but also with the temperature at which the eutectoid reaction takes place, which itself is sensitive to cooling rate. Hence it is appropriate to rewrite Equation 5a in terms of fraction of austenite, pro-eutectoid ferrite $x^{\alpha,\mathrm{pro}}$ and pearlite x^p

$$x^\gamma + x^{\alpha,\mathrm{pro}} + x^p = 1 \quad (5b)$$

In this case, Equation 1 becomes

$$C_p = x^\gamma C_p^\gamma + x^{\alpha,\mathrm{pro}} C_p^\alpha + x^p C_p^p + \frac{dQ}{dT} \quad (6)$$

where dQ/dT includes both the heat of formation of pro-eutectoid ferrite and the heat of formation of pearlite. After some rewriting, it follows that

$$\frac{dx^p}{dT} = x^p \frac{C_p^\gamma - C_p^p}{\Delta H^p} - \frac{(1 - x^{\alpha,\mathrm{pro}})C_p^\gamma + x^{\alpha,\mathrm{pro}} C_p^\alpha + \Delta H^{\alpha/\gamma} \dfrac{dx^{\alpha,\mathrm{pro}}}{dT} - C_p}{\Delta H^p} \quad (7)$$

where ΔH^p is the enthalpy of formation of pearlite from austenite. In this equation, the heat capacities and the enthalpies of formation of the various phases are allowed to be temperature dependent. Equation 7 is used to analyse the heat effects of the pearlite formation whereas Equation 4 is used to analyse the heat effects when only a single process is to be considered (i.e. pro-eutectoid ferrite formation).

To solve Equation 7 for x^p, it is required to prescribe $x^{\alpha,\mathrm{pro}}$ during the eutectoid reaction. The first approximation one could use is to take the value of $x^{\alpha,\mathrm{pro}}$ during the eutectoid reaction as constant and equal to the value it had just before the onset of the eutectoid reaction. However, as will be shown in this paper, the formation of pro-eutectoid ferrite and pearlite are competing processes and hence $x^{\alpha,\mathrm{pro}}$ changes during the eutectoid reaction. It was therefore chosen to use a linear extrapolation of $dx^{\alpha,\mathrm{pro}}/dT$ from the value at the onset of the eutectoid reaction to zero at the end of the transformation yielding a quadratic behaviour of $x^{\alpha,\mathrm{pro}}$ during the eutectoid reactions. This approximation is considered to be sufficient as far as the fraction $x^{\alpha,\mathrm{pro}}$ does not vary too much during pearlite formation. In the case the alloy composition is close to the eutectoid composition (e.g. Fe–0.6% C) this approximation will not be correct. The solution of Equation 7 is therefore subject to the boundary constraints at the start of the eutectoid reaction $x^p = 0$ and the value of $dx^{\alpha,\mathrm{pro}}/dT$ which follows from the solution of Equation 4.

Both Equation 4 (pro-eutectoid ferrite formation) and Equation 7 (ferrite and simultaneous pearlite formation) are easily solved numerically by using the trapezoid rule. An integration interval of 1 K was used. Numerical stability problems were not encountered. All integrations were performed from high temperature downwards. For the calculation of the pro-eutectoid ferrite formation (i.e. the solution of Equation 4), the boundary condition $x^\gamma = 1$ at the start of the transformation was used.

It should be pointed out explicitly that in this work pro-eutectoid ferrite is not defined as the ferrite formed before the start of the pearlite formation but as the ferrite not forming part of the pearlitic part of the microstructure.

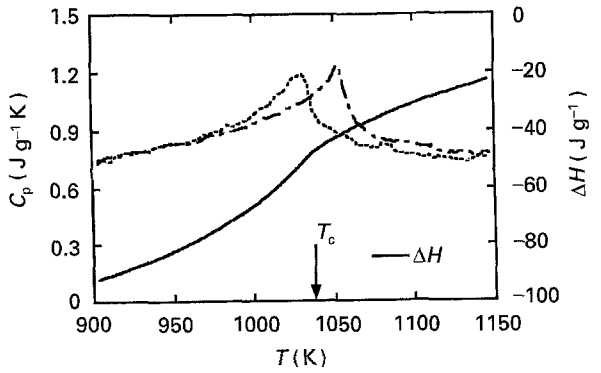

Figure 1 The measured heat capacity for ferrite C_p^{α} in pure iron. The experiments were performed at a scanning rate of 20 K min^{-1}. Also the enthalpy difference between ferrite and austenite is given as a function of temperature (solid line).

2.2. Parameter evaluation

To solve Equations 4 and 7, the temperature dependence of the heat capacities and the enthalpies of formation of the various phases should be known accurately. As this information is essential, for the analysis, the specific details for these input data will be described in detail first.

2.2.1. Heat capacity of austenite

The heat capacity of austenite is assumed to be a linear function in the temperature range of interest. It can therefore be determined by linear extrapolation from the temperature range in which the austenite is stable. For this purpose, the heat capacity data of a eutectoid alloy in its austenitic state are used. For dilute Fe–C alloys like those used in this work, the heat capacity of austenite was found to be independent of the carbon content (cf. Fig. 2).

2.2.2. Heat capacity of ferrite

During continuous cooling of Fe alloys at a rate of 20 K min^{-1}, the maximum of the heat capacity due to the ferromagnetic transition is observed at 1023 K. On continuous heating at the same rate, this peak is found at a temperature of approximately 1052 K. The value accepted in the literature for the Curie temperature T_c is approximately 1043 K. Considering the cooling rate used, this peak shift is too large to be explained by a temperature lag of the sample with respect to the thermocouple*. Also, the temperature calibration of the thermocouples has been examined and was found to be correct (calibration points reproducing within 0.3 K). Since the solution of Equation 4 is sensitive to errors in C_p^{α}, the measured values for ferrite have been used instead of values given in literature (e.g. [4, 5]). Due to the low solubility of carbon in ferrite, the heat capacity of ferrite does not depend on the alloy carbon content.

2.2.3. Heat capacity of pearlite

The value of C_p^p may be found by measuring the heat capacity of a sample with eutectoid composition. This yields a C_p with an average carbon concentration of 0.8%. However, as mentioned before, in the case of hypo-eutectoid Fe–C alloys, the average carbon concentration in pearlite may be lower, depending on the cooling rate. Hence, the heat capacity of pearlite may vary from one case to another. A more suitable approach is to determine C_p^p from the heat capacity measurements at completed transformation. This can be done by choosing a value of C_p^p so that the left hand side of Equation 7 vanishes at completed transformation, implying

$$C_p^p = \frac{C_p - x^{\alpha,\mathrm{pro}} C_p^{\alpha}}{1 - x^{\alpha,\mathrm{pro}}} \quad (8)$$

In this work, C_p^p for hypo-eutectoid alloy compositions during the pearlite formation is determined by multiplying C_p^p for the Fe–0.8 mass % C alloy with an adjustable constant. This constant is adjusted such that dx^p/dT vanishes at completed transformation. Note however, that this procedure is very susceptible to experimental errors at low pearlite fractions.

2.2.4. Enthalpy of formation of pro-eutectoid ferrite

The enthalpy difference between ferrite and austenite $\Delta H^{\alpha/\gamma}$, which has been determined by integration of the heat capacity of ferrite while taking the literature value of $\Delta H^{\alpha/\gamma}$ at 630 K [5] as a reference point (i.e integration constant). The result is given in Fig. 1. The strong increase of the enthalpy difference with decreasing temperature is, to a large extent, caused by the ferromagnetism of ferrite. Since the heat capacities of both ferrite and austenite do not depend on the carbon content, $\Delta H^{\alpha/\gamma}$ is not a function of the alloy carbon content.

2.2.5. Enthalpy of formation of pearlite

Also the enthalpy of pearlite formation ΔH^p is not known in advance and has to be determined from these measurements. Because the eutectoid reaction takes place over a limited temperature range, ΔH^p is considered to be constant. The value of ΔH^p can be determined by taking into account the value $x^{\alpha,\mathrm{pro}}$ at the onset of pearlite formation, the behaviour of $x^{\alpha,\mathrm{pro}}$ during the reaction and the fact that the material must be completely transformed when the process is finished (ie. $x^{\alpha,\mathrm{pro}} + x^p \equiv 1$ at the end of the reaction).

*Analysis of the variation of the onset temperature of the α/γ transformation in pure Fe with the heating/cooling rate reveals that a temperature shift of no more than 4 K can be expected at the cooling rate used. However, in the temperature range of interest, an analysis of temperature lag should be performed using the melting points of pure metals as defined by the temperature scale ITS 90 (see Ref. [6] for a discussion on this subject). Therefore, a temperature shift of 4 K is an overestimation of the instrumental effects in the observed shift of the ferromagnetic contribution in C_p^{α}. These results were obtained using a Netzsch DSC 404 and were confirmed by repeating the measurement using a Perkin Elmer DTA-7.

TABLE I Chemical composition in mass % of the Fe–C alloys employed, as determined by inductively coupled plasma optical emission spectroscopy or atomic absorption spectroscopy

Element/ Name	C	S	P	Cr	Mn	Ni	Cu	Mo	Sn
Fe	0.01	< 0.005	< 0.001	0.001	0.0007	0.003	0.001	0.0002	0.002
Fe–0.17 C	0.17	< 0.005	< 0.001	0.001	0.0007	0.004	0.007	0.0007	0.001
Fe–0.36 C	0.36	< 0.005	< 0.001	0.001	0.0007	0.003	0.015	0.0003	0.001
Fe–0.57 C	0.57	< 0.005	< 0.001	0.001	0.0009	0.001	0.002	0.0018	0.001
Fe–0.8 C	0.80	< 0.005	0.038	0.0002	0.0005	0.003	0.006	0.0005	0.003

3. Experimental procedure

The formation of pro-eutectoid ferrite and pearlite from an austenite matrix was studied using various hypo-eutectoid Fe–C alloys. The alloys were prepared by arc melting iron, with the chemical composition as indicated in Table I, under an argon flow while adding pure graphite to obtain the carbon concentration required. Austenitizing took place at 1273 K for 15 min, after which the solid alloy was hot-rolled to a thickness of 4 mm. The chemical composition after hot-rolling was determined using inductively coupled plasma optical emission spectroscopy or atomic absorption spectroscopy and is listed in Table I. The rolled slabs were annealed yielding a microstructure of spherical cementite particles (diameter 2 μm) in a ferrite matrix.

With the exception of the Fe–0.8 mass % C alloy, the specimens where produced by cold-rolling of the material to a thickness of approximately 0.3 to 0.5 mm and by punching out a sample with a diameter of 6 mm. The sample surfaces where cleaned by abrading the surface and subsequent cleaning with alcohol. The sample of the eutectoid alloy was produced by preparing a cylindrical rod with a diameter of 6 mm on a lathe. From this rod, slices with a thickness of approximately 0.5 mm where prepared using a diamond blade saw.

The calorimetric measurements where carried out using a Netzsch DSC 404 (heat-flux type), using S-type thermocouples and platinum crucibles, covered with a platinum lid to avoid differences in radiation and convection losses between the sample and reference materials at high temperatures. Argon was used to provide a protective atmosphere (flow 50 ml min^{-1}). The heat treatment received by the samples is as follows. The samples are inserted in the apparatus at ambient temperature. Next, the temperature is raised to 870 K (rate programmed to 100 K min^{-1}). After 3 min equilibrating the DSC cell, the temperature programme continued with heating at a constant rate of 20 K min^{-1} to 1270 K. The sample was held at this temperature for 5 min to enable the carbon to attain a uniform distribution throughout the sample. The austenitizing time is relatively short to avoid decarburizations as much as possible, which can easily occur in an argon atmosphere at these temperatures. Next, the sample was cooled at a constant rate of 20 K min^{-1}. During this part of the temperature program, the formation of ferrite from the austenite matrix can be studied. An identical temperature programme was followed with empty crucibles, to enable the correction for instrumental contributions to the measured heat flow (the so-called baseline). Also, a sapphire has been subjected to this temperature programme, yielding the reference signal. The heat capacity of sapphire (α-corundum) is well established in literature [7]. The baseline was subtracted from both the sapphire run and the sample run. Taking the subtracted sample line and the subtracted sapphire line, the heat capacity of the sample was determined using (see e.g. [8]).

$$C_P = \frac{m_{ref}}{m_{sample}} \frac{\Delta U_{sample}}{\Delta U_{ref}} C_P^{ref} \quad (9)$$

where C_P is the heat capacity of the sample, m_{ref} and m_{sample} are the masses of the reference sapphire and sample respectively, while ΔU_{sample} and ΔU_{ref} are the subtracted DSC output signals of the sample and reference sapphire respectively, given as either the temperature differences or the thermocouple voltage differences. For heat-flux DSC, this equation can be shown to hold in case of relatively slow transformation kinetics with moderate heat-effects (see discussion in [1]).

The fractions of pro-eutectoid ferrite at completed transformation can be verified by examination of the microstructure using quantitative image analysis. The cooling rates in the DSC are relatively low and hence the samples are exposed to relatively high temperatures for relatively long times. This may alter the microstructure after completed transformation, in particular in pearlitic part of the microstructure. To circumvent this problem, cylindrical thin walled specimens of the same alloy compositions are subjected to an identical heat-treatment as used in the DSC-experiments, but now using a dilatometer with a quenching facility. At a temperature of approximately 910 K, i.e. when the transformation was just completed, the specimen was quenched to room temperature. This procedure ensures that after completed transformation, the microstructure had not changed significantly due to exposure of the specimen to high temperatures for longer times. For temperature measurement and control, S-type thermocouples are spot-welded on the outer surface of the sample. The sample is kept in position using quartz pushrods. The thermocouple is positioned at the central part of the sample. Although the thermal conductivity of quartz is extremely low as compared to iron and steel (in particular at the temperatures considered), the existence of a small temperature drop at the contact surface between the

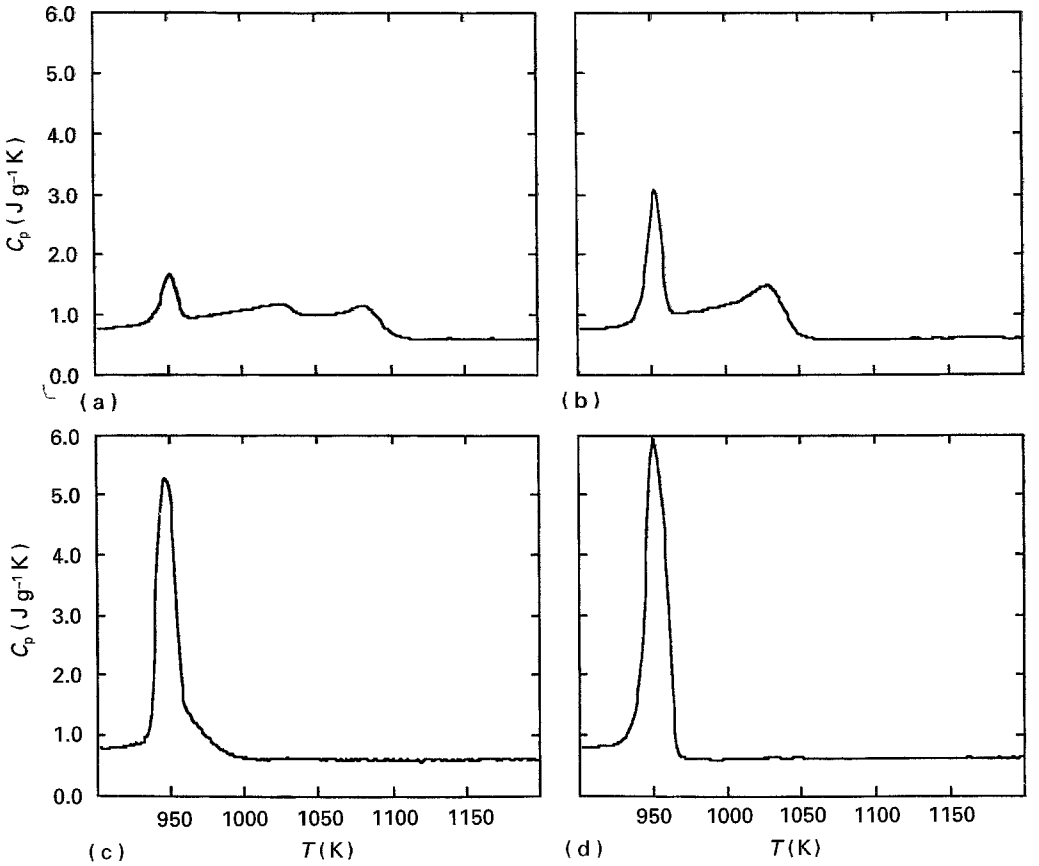

Figure 2 Heat capacities of the various Fe–C alloys at a cooling rate of 20 K min^{-1} (a) Fe–0.17 mass % C; (b) Fe–0.36 mass % C; (c) Fe–0.57 mass % C; (d) Fe–0.8 mass % C.

pushrod and the sample cannot be ruled out. Therefore the sample has been cut in the vicinity of the thermocouple. This cross-section has been examined. The analysis of the microstructure was performed using a Leitz CBA 8000 quantitative image analysis system. The area fraction pro-eutectoid ferrite as determined using a quantitative image analysis as to be compared with the mass fraction pro-eutectoid ferrite as determined from DSC.

4. Results

4.1. Heat capacity measurements

The heat capacities, C_p, for the various alloys during continuous cooling at a rate of 20 K min^{-1} are given in Fig 2. The figure shows that the α/γ phase transformation starts at a temperature that decreases with carbon content. The starting temperatures are in agreement with the A_3 temperatures of the Fe–C diagram.

The behaviour during the phase transformation is different for each composition. The C_p curve of sample containing 0.17 mass % carbon shows three peaks. The first peak occurring on cooling from the austenite region can be identified as the start of the α/γ transformation. The second peak is mainly caused by the ferromagnetic transition of the ferritic part of the sample. This heat effect is part of the heat capacity of ferrite already formed and illustrates the non-linearity of the heat capacity of the sample. The third peak is a consequence of the occurrence of the eutectoid reaction $\gamma \rightarrow \alpha + \theta$, during which not only ferrite but also cementite forms. During this process, the formation of pro-eutectoid ferrite continues. The C_p curve of the sample containing 0.36 mass % carbon shows two peaks. On cooling from the austenite region, the first peak contains a significant contribution from the ferromagnetic transition as well as from the α/γ transformation. The second peak, due to the eutectoid reaction, is more pronounced than was the case with the 0.17 mass % alloy. This is due to the fact that the amount of pearlite formed increases with the carbon content. The C_p curve of the alloy containing 0.57 mass % carbon shows only one peak. The formation of pro-eutectoid ferrite is only visible from the difference in the slope of the peak in the first stages of the process. However, the major part of the process consists of the eutectoid reaction. A small part of the heat effects can be attributed to the ferromagnetic transition. The transformation which occurs in Fe–0.8 mass % C alloy is considered to consist of only one process: pearlite formation.

4.2. Determination of fractions transformed

Fig. 3 shows the formation of pro-eutectoid ferrite per unit of temperature for the Fe-0.17 mass % C and Fe–0.36 mass % C alloys as determined using Equation 4 (see also Section 2.3). It is clear that $dx^{\alpha,pro}/dT$ is non-zero at the start of the pearlite formation indicating that the formation of pro-eutectoid ferrite continues during pearlite formation. Fig. 4 gives the

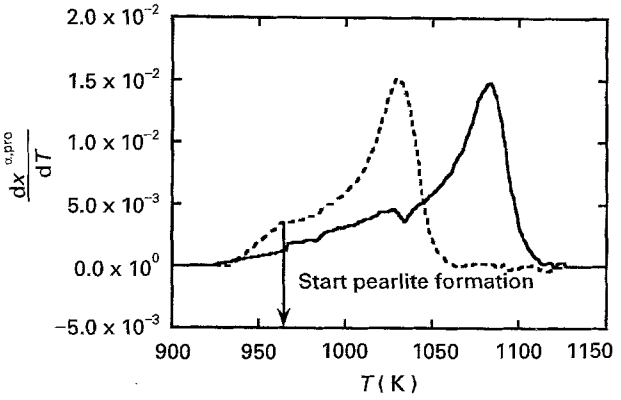

Figure 3 Formation of pro-eutectoid ferrite per unit of temperature for the Fe–0.17 mass % C (—) and Fe–0.36 mass % C (– – –) alloys.

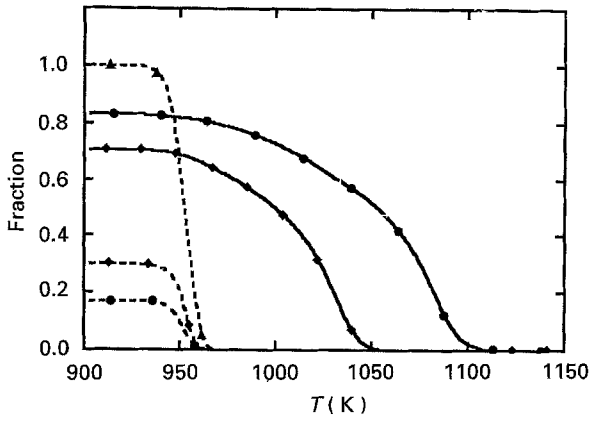

Figure 4 Calculated fractions of pro-eutectoid ferrite and pearlite as a function of the temperature for Fe–0.17 mass % C, Fe–0.36 mass % C and Fe–0.8 mass % C alloys at a cooling rate of 20 K min^{-1}. –●– $x^{\alpha,pro}$ (0.17 mass % C); –●– x^{p} (0.17 mass % C); –◆– $x^{\alpha,pro}$ (0.36 mass % C); –◆– x^{p} (0.36 mass % C); –▲– x^{p} (0.8 mass % C).

fractions $x^{\alpha,pro}$ and x^{p} as a function of temperature for the alloys Fe–0.17 mass % C, Fe–0.36 mass % C and Fe–0.8 mass % C.

The pearlite fractions for the Fe–0.17 mass % C and Fe–0.36 mass % C alloys have been determined using Equation 7 and adjusting the values of C_p^p and ΔH^p (cf. Sections 2.2.3 and 2.2.5).

The transformation in the Fe–0.8 mass % C alloy consists of a single process (the eutectoid reaction). It is therefore analysed using Equation 4. The heat capacity of pearlite has been used instead of the heat capacity of ferrite. The heat capacity of pearlite in the temperature range of interest, determined from the measurement of Fe–0.8 mass % C after completed transformation, can be described as

$$C_p^p = -0.948 + 1.923 \times 10^{-3} T \ (J g^{-1} K) \quad (10)$$

The enthalpy of pearlite formation was estimated using the constraint that the austenite fraction must drop from 1 at the start of the process to 0 at the end of the transformation.

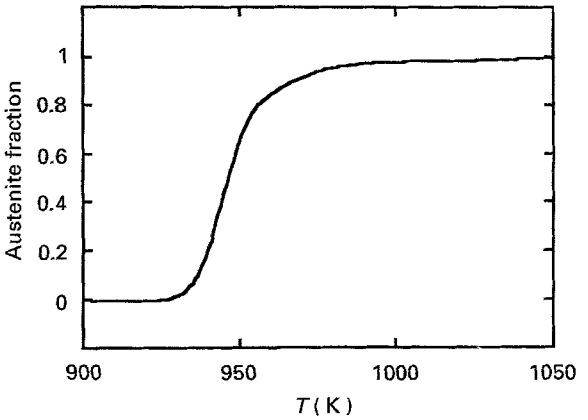

Figure 5 Calculated austenite fraction as a function of the temperature for the Fe–0.57 mass % C alloy.

TABLE II The estimated enthalpy of pearlite formation from austenite ΔH^p for the different alloys. ΔH^p is determined by parameter optimization and the boundary constraints as described in the text. Also the ratio of the heat capacity of pearlite for the various alloy carbon compositions with respect to the eutectoid composition is given

Mass % C	ΔHp (J g^{-1})	C_p^p/C_p^p (0.8 mass % C)
0.17	64	0.32
0.36	83	0.55
0.57	85	0.94
0.8	85	1

Analysis of the heat effects of the transformation of the Fe–0.57 mass % C alloys involves a difficulty insofar as there is no clear distinction between the formation of pro-eutectoid ferrite and pearlite. The heat effects were analysed using Equation 4, thus treating the transformation as a single process. For the tC_p and ΔH values, the data of pure ferrite and pure austenite have been used. The austenite fraction x^{γ} is found to drop from 1 to 0 within 2% accuracy (see Fig. 5). Apparently, the difference between the heat capacities of ferrite and pearlite is very small, while there is also no distinction between the enthalpy of formation of pearlite from austenite and the enthalpy of formation of ferrite from austenite at these temperatures and for the alloy composition considered.

The estimated enthalpy of formation of pearlite and the heat capacities of pearlite are given in Table II for the various alloy compositions.

The results of the calorimetric experiments were verified by examination of the microstructure after completed transformation using quantitative image analysis (cf. Section 3). The results are listed in Table III. For comparison, the corresponding fractions as found by analysis of the heat effects and the maximum amount of pro-eutectoid ferrite that can form according to the equilibrium phase diagram are also included.

4.3. Overlapping reactions

Proof for the statement of simultaneous pearlite and pro-eutectoid ferrite formation is found if the transformation is interrupted during pearlite formation and

TABLE III Fractions of pro-eutectoid ferrite at completed transformation based on the phase diagram, DSC measurements and quantitative analysis of the microstructure respectively. Data at 960 K apply to partially transformed samples

Mass % C	$x^{\alpha,pro}$ (equilibrium) $T = 1000$ K	$x^{\alpha,pro}$ (DSC) $T = 910$ K	$x^{\alpha,pro}$ (image analysis)	
			$T = 960$ K	$T = 910$ K
0.17	0.81	0.82	0.82	0.86
0.36	0.56	0.71	0.49	0.72
0.57	0.29	–	–	0.1

the microstructure is examined. For this purpose, the procedure as described for the quantitative image analysis measurements has been repeated. The temperature for the start of the quench to ambient temperature was chosen such that the eutectoid reaction was interrupted (approximately 940 K), thus invoking a martensitic transformation in the remaining austenite. An example of the resulting microstructure is given in Fig. 6. The microstructure reveals the presence of both ferrite/martensite interfaces and pearlite/martensite interfaces. It appears that not all possible sites for pearlite nucleation are occupied and it may well be that growth of the ferrite particles continues at such unoccupied sites. Quantitative evidence is found by examination of the microstructure just before the start of the pearlite reaction. This microstructure is obtained by repeating the procedure but starting the quench to room temperature at approximately 960 K. Quantitative image analysis revealed a significantly lower value of the fraction pro-eutectoid as compared to the result at completed transformation (compare the last two columns in Table III). In particular, at higher alloy carbon contents, the overlap between both processes is not negligible.

5. Discussion

In the preceding sections it was shown that the heat effects occurring on continuous cooling of hypo-eutectoid Fe–C alloys from the region of austenite stability can be separated into instrinsic heat capacity and heat of transformation effects. The latter is proportional to the amount of transformation per unit of temperature, which itself is directly proportional to the transformation rate. The method described in Section 2 has been used to convert the measured heat capacity into the fractions pro-eutectoid ferrite and pearlite as a function of temperature. The results are the smooth S-shaped curves given in Fig. 3. Pro-eutectoid ferrite formation is analysed using the heat capacities as measured for the Fe–C alloys, pure ferrite and pure austenite and the enthalpy difference between ferrite and austenite, all of which are temperature dependent. The results are subject only to the boundary constraint that the sample must be completely austenitic at the start of the transformation. No parameter adjustment is required. The fractions of pro-eutectoid ferrite at completed transformation as found from the

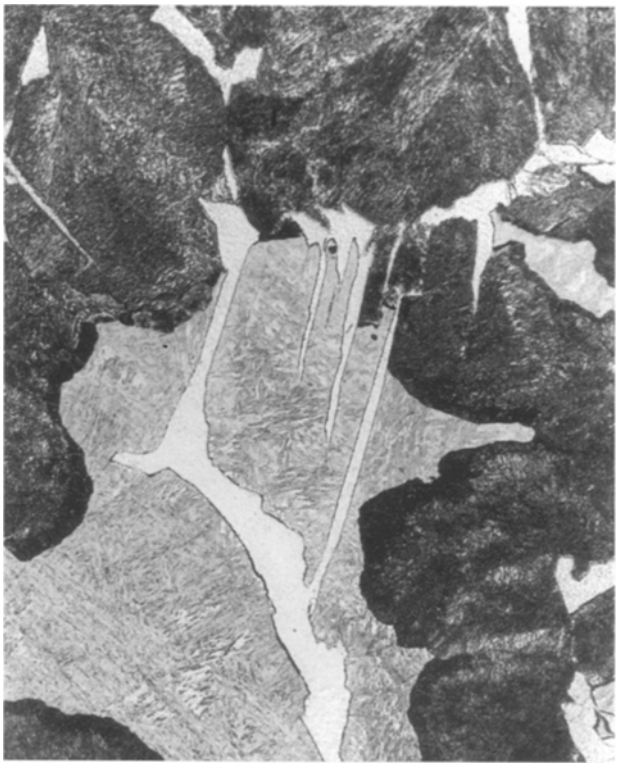

Figure 6 Microstructure of a Fe–0.57 mass % C alloy quenched from 940 K after cooling at a rate of 20 K min^{-1} from a temperature of 1270 K, showing ferrite, pearlite and martensite.

analysis of the heat effects agrees well with that found by quantitative image analysis. From this point of view, the results are considered reliable. The amount of pro-eutectoid ferrite as determined from DSC and quantitative image analysis (cf. Table III) in the Fe–0.17 mass % C alloy is in agreement with the value calculated on the basis of the Fe–C phase diagram. For the Fe–0.36 mass % C alloy, the fractions of pro-eutectoid ferrite determined experimentally however are larger than the value calculated from the phase diagram. The reason for this is not clear.

To meet the constraint $x^{\gamma} = 0$ and $x^{\alpha,pro} + x^{p} = 1$ at the end of the transformation, an adjustment of the enthalpy of formation of pearlite from austenite and the heat capacity of pearlite is necessary. Except for the Fe–0.17 mass % C alloy, the values for ΔH^{p} for the different alloy composition agree and $\Delta H^{p} = 85\ J\ g^{-1}$ seems to be a reliable value. The results for C_p^p, however, are considered to be less reliable. Considering that the heat capacity of cementite [9] is lower than that of ferrite and that the amount of cementite contained by the sample increases with increasing alloy carbon content, a decrease of the measured alloy heat capacity, C_p, with increasing alloy carbon content is expected at completed transformation. No such relation between C_p at these temperatures and the alloy carbon content is found. Hence C_p^p must increase with increasing alloy carbon content. This result however is related to a small heat effect, in particular at low carbon contents. Also C_p^p is one of the very few adjustable parameters. Therefore this result is more susceptible to experimental and numerical errors than any of the other parameters determined.

At the start of pearlite formation $dx^{\alpha,pro}/dT$ is non zero, indicating that the formation of pro-eutectoid ferrite might continue during pearlite formation. This conclusion is supported by the results of quantitative image analysis given in Table III. Considering the amount of pro-eutectoid ferrite already formed at the start of pearlite formation, it may be concluded that the formation of pro-eutectoid ferrite continues during pearlite formation mainly by growth of existing pro-eutectoid ferrite particles at those austenite/ferrite interfaces where the conditions for the start of pearlite formation have not been met. However, the Widmanstätten ferrite present in the microstructure of the Fe–0.57 mass % C alloy, as given in Fig. 6, is known to appear at lower temperatures, in particular those at which pearlite formation occurs [10]. For this alloy composition, a large part of the overlap between the formation of pro-eutectoid ferrite and pearlite is caused by nucleation and growth of ferrite particles in the form of Widmanstätten ferrite. No signs of Widmanstätten ferrite were found in the Fe–0.17 mass % C and Fe–0.36 mass % C alloys. The formation of pro-eutectoid ferrite during the pearlite formation is therefore considered to be caused by growth of existing ferrite particles at those interfaces not occupied by pearlite. This explains the relatively small overlap at these alloy carbon contents. Based on the considerations given above, it must be concluded that a part of the heat-effects occurring during the pearlite formation must be attributed to the transformation $\gamma \rightarrow \alpha$. The difference in enthalpy of formation for pro-eutectoid ferrite and pearlite from the austenite matrix at this temperature range is small (see also Fig. 1). For the Fe–0.57 mass % C alloy, this makes an accurate separation between the effects due to pro-eutectoid ferrite formation and pearlite formation mostly impossible.

6. Conclusions

A method has been presented to study phase transformations and reactions using differential scanning calorimetry, even when the heat effects depend on the temperature at which the transformation takes place. The heat effects due to the phase transformation can be separated from the intrinsic heat capacity effects, allowing the determination of the fraction transformed as a function of the temperature. This method has been applied to the transformation $\gamma \rightarrow \alpha(+\theta)$ in Fe–C alloys. For the lower alloy carbon contents, a clear distinction between the formation of pro-eutectoid ferrite and pearlite is found, as far as the range of temperatures and heat effects is concerned. With increasing carbon content an increasing of overlap of these processes occurs, as determined from analysis of both the heat-effects and the microstructure. In near-eutectoid Fe–C alloys, this effect is very pronounced. The enthalpy of formation of pearlite is found to be $85\ J\,g^{-1}$, at least for the higher alloy carbon contents.

Acknowledgements

The authors are grateful for financial support from the Innovative Development Project for Metals of the Dutch Ministry of Economic Affairs (IOP-Metalen) and for the financial and experimental support by Hoogovens Corporate Research, IJmuiden, The Netherlands. The authors are particularly indebted to Miss Karina v.d. Vliet of the Hoogovens Ceramic Research Centre for her skilful assistance with the calorimetric experiments.

References

1. W. F. HEMMINGER and H. K. CAMMENGA, "Methoden der Thermischen Analyse" (Springer Verlag, Berlin, 1989) p. 100.
2. R. F. SPEYER, in "Thermal analysis of materials" (Marcel Dekker Inc., New York, 1994) p. 75.
3. H. J. BORCHARD and F. DANIELS, *J. Amer. Chem. Soc.* **79** (1957) 41.
4. W. BENDICK and W. PEPPERHOFF, *Acta Metall.* **30** (1982) 679.
5. R. L. ORR and J. CHIPMAN, *TMS-AIME* **239** (1967) 630.
6. G. W. H. HÖHNE, H. K. CAMMENGA, W. EYSEL, E. GMELIN and W. F. HEMMINGER, *Thermochim. Acta* **160** (1990) 1.
7. J. D. COX, *Pure & Appl. Chem.* **40** (1974) 419.
8. R. F. SPEYER, in "Thermal analysis of materials" (Marcel Dekker Inc., New York, 1994) 79.
9. I. BARIN and O. KNACKE, "Thermochemical properties of inorganic substances" (Springer Verlag, Berlin, 1973) p. 301.
10. D. A. PORTER and K. E. EASTERLING, "Phase transformations in metals and alloys" (Chapman & Hall, London, 1981) p. 320.

Received 19 October 1994
and accepted 8 September 1995